metals

MDPI

Article

New Method to Recover Activation Energy: Application to Copper Oxidation

Dominique Barchiesi *,† **and Thomas Grosges** †

Automatic Mesh Generation & Advanced Methods (GAMMA3), University of Technology of Troyes, 12 rue Marie Curie, CS 42060, 10004 Troyes CEDEX, France; thomas.grosges@utt.fr

* Correspondence: dominique.barchiesi@utt.fr

† These authors contributed equally to this work.

Abstract: The calculation of the activation energy helps to understand and to identify the underlying phenomenon of oxidation. We propose a new method without any a priori hypothesis on the oxidation law, to retrieve the activation energy of partially and totally oxidized samples subject to successive annealing. The method handles the uncertainties on the measurement of metal and oxide thicknesses, at the beginning and at the end of the annealing process. The possible change in oxidation law during annealing is included in the model. By using an adapted Particle Swarm Optimization method to solve the inverse problem, we also calculate the time of final oxidation during the last annealing. We apply the method to successive annealings of three samples with initial nanometric layers of copper, at ambient pressure, in the open air. One, two and three successive laws are recovered from experimental data. We found activation energy values about 105–108 kJ mol^{-1} at the beginning of the oxidation, 76–87 kJ mol^{-1} at the second step, and finally 47–59 kJ mol^{-1} in a third step. We also show that the time evolution of copper and oxide thicknesses can also be retrieved with their uncertainties.

Keywords: metallic thin films; activation energy; copper; copper oxide; oxidation law; Arrhenius law; Particle Swarm Optimization method

Citation: Barchiesi, D.; Grosges, T. New Method to Recover Activation Energy: Application to Copper Oxidation. *Metals* **2024**, *14*, 1066. https://doi.org/10.3390/met14091066

Academic Editor: Koh-ichi Sugimoto

Received: 10 July 2024
Revised: 29 August 2024
Accepted: 29 August 2024
Published: 18 September 2024

1. Introduction

Copper and copper oxides are widely used for ultralarge-scale-integration devices because of its remarkable electric conductivity [1]. They have a wide range of applications in electronic devices like solar cells and sensors as well as in the field of catalysts, batteries, taking advantage of the band gap energies of oxides (from 1.2 to 2.1 eV) [2–5]. Copper is known to oxide even at room temperature. Copper oxides belong to transition metal oxides that are an important classes of semiconductors. This oxidation could may be considered as an advantage or as a problem in nano-science, as it strongly modifies the plasmonic properties [6]. In addition, they have significantly different properties at the nanometer length scale from their bulk materials [7,8]. Therefore, many studies focused on copper oxidation for a better understanding of the mechanism governing this phenomenon, as a function of temperature and pressure, especially for thin oxide layers. The activation energy and the oxidation law deserve to be determined for thin copper films as it may help to reveal the specificity of the mechanism of oxidation [9].

A careful discussion on the underlying phenomenons of copper oxidation (step edges and surface structure) can be found in Refs. [10,11]. The lattice diffusion of copper ions at the interface favors the formation of Cu_2O phase whereas grain boundary diffusion favors the formation of CuO phase. The diffusion of oxygen into the bulk and copper towards the free surface occurs along the defects of oxide [12]. Under ambient air pressure and below 520 K only Cu_2O was found to be thermodynamically stable [7,13,14]. Ellipsometry measurements revealed Cu_2O oxidation layer in air, at 398 K [15]. The oxide film was

mostly Cu_2O, and CuO developed at 300 K [16], after several days at 373 K or at higher temperature (above 600 K) [7,17] or by specific chemical process, deposition mode and annealing [18–20]. In the present study, the annealing temperature is lower than 450 K [8]. Therefore, it is reasonable to assume a single oxide layer.

The objective is the calculation of the activation energy, from successive annealings of the same initial sample, at ambient air pressure and at controlled temperature. The classical methods used to calculate the activation energy from experiments are directly based on the fitting of the oxidation rate using measurement of thicknesses, as a function of the inverse of temperature, assuming a given oxidation law. The main drawbacks of the classical method are following.

- The systematic measurement of thicknesses may be destructive, it is also subject to uncertainties and is depending on the method of measurement [21].
- The choice of the fitting function is often based on preliminary hypothesis on the oxidation mechanism [22–24].
- The detection of the possible change of oxidation law is based on visual inspection of the change of slope of the oxidation rate.
- The fitting does not handle the uncertainties of measurement of oxide thicknesses.
- The time of the full oxidation of copper cannot be retrieved.

To overcome these drawbacks as much as possible, we propose a new method to determine the activation energy. This method has the following properties:

- to prevent oxide and copper damage by excessive manipulations especially for thicknesses measurements, we suppose that the thicknesses are only measured only for both the initial copper sample (after deposition) and the final sample (after full oxidation). Therefore the intermediate thicknesses must be evaluated numerically.
- No a priori hypothesis is made on the oxidation law.
- The possible changes of the oxidation law during the successive annealings are numerically detected and the oxidation time at which it occurs is calculated.
- The proposed method handles the uncertainties on the initial and final oxide thicknesses.
- The time at which the complete copper oxidation takes place can be retrieved.

To achieve these goals, we consider the activation energy as the solution of an inverse problem instead of simply the result of a fitting of experimental data. Such inverse problem resolution necessitates more numerical evaluations than a simple fitting of data to a given model of oxidation.

This paper is organized as follow. Sections 2 and 3 presents the method of resolution of the inverse problem and the considered models of oxidation. Section 4 gives insights on the investigated experimental data. Section 5 gives the numerical results of the resolution of the inverse problem from experimental data and proposes a discussion, before concluding. The tuning of the numerical method used to solve the inverse problem, the experimental techniques to elaborate the samples and the calculation of uncertainties on the activation energy are given in Appendices A, B and C, respectively.

2. The Inverse Problem

The inverse problem consists in finding the unknowns in the model, to best fit the experimental data. These unkwowns are inputs of a physical model. In the present study, oxidation models that are solutions of the kinetic equation are under consideration. These models relate annealing time and temperature, thickness of oxide or metal, and the activation energy through the Arrhenius law [25]. From measured initial thicknesses of metal and oxide, the successive ones are calculated iteratively, for each annealing of the sample. The first thicknesses are subject to uncertainties. According to literature [1], different physical phenomenons govern the oxidation, depending on the oxide thickness (diffusion of oxygen and of metal ions, tunneling effect, electrostatic attraction, structure and side effects of oxide…). Therefore, in this study, we suppose that two or three different oxidation laws can describe the full oxidation process, but we do not made any preliminary

physical hypothesis underlying the oxidation phenomenon. The principle of the method is the repeated realization of the same algorithm:

1. Random draw of initial thicknesses of copper and oxide in their uncertainty interval.
2. The direct calculation of the final thickness of copper and oxide from the model. The model parameters are the time of complete oxidation (the complete oxidation of the sample occurs during the last annealing of the sample.), the parameters of oxidation laws (including the activation energies) and the annealing for which the oxidation law changes.
3. The acceptable solution must verify that the final thicknesses of copper $\left(m\left(h_{end}^{Cu}\right)\right)$ and oxide $\left(m\left(h_{end}^{Ox}\right)\right)$ belong to the interval of uncertainty of their measurement.
   - If this condition is fulfilled, the parameter set is considered as possible and is kept for further descriptive statistics analysis.
   - If not, the parameters of the model are adjusted using the closeness of the copper and oxide thicknesses to the interval of uncertainty of their measurement (the solution quality).

The numerical solutions are acceptable only if the oxide thickness increases, the metal one decreases. To solve the inverse problem, we define the following fitness function that should be minimized:

$$F = \begin{cases} 0 & \text{if} \quad h_{end}^{Cu} \in I_{m\left(h_{end}^{Cu}\right)} \text{ and } h_{end}^{Ox} \in I_{m\left(h_{end}^{Ox}\right)} \\ \sqrt{\left(1 - \frac{h_{end}^{Cu}}{m\left(h_{end}^{Cu}\right)}\right)^2 + \left(1 - \frac{h_{end}^{Ox}}{m\left(h_{end}^{Ox}\right)}\right)^2}, & \text{elsewhere,} \end{cases} \tag{1}$$

where the calculated final thicknesses of copper and oxide are h_{end}^{Cu} and h_{end}^{Ox} respectively, the measured ones being $m\left(h_{end}^{Cu}\right)$ and $m\left(h_{end}^{Ox}\right)$. The intervals of uncertainty of these measurements are $I_{m\left(h_{end}^{Cu}\right)}$ and $I_{m\left(h_{end}^{Ox}\right)}$. This definition of the fitness function prevents artificial attraction of the solution to the mean value of the measured values.

The most flexible algorithms to solve this inverse problem are the metaheuristic optimization methods [26]. We use the Particle Swarm Optimization method (PSO) [27]. We already successfully used this method to recover the materials and particle size in the Lycurgus cup from colors in photographs [28] or thicknesses and optical properties of bilayers of copper and oxide [8]. In this paper, we tune PSO to ensure the conditions of iterative convergence of the algorithm (Appendix A).

3. Model for Oxidation

Experimentally, various oxidation laws were found (logarithmic (Log), inverse-logarithmic (Ilg), quartic (Qua), cubic (Cub), parabolic (Par) and linear (Lin)) [29]. In this section, we show that these oxidation laws are solutions of the kinetic law and we summarize the underlying physical phenomenons for each of them.

The evolution of oxide thickness h^{Ox} as a function of oxidation time t is solution of the following kinetic differential equations:

$$\frac{dh^{Ox}}{dt} = k \cdot g(t) \cdot f(h^{Ox}), \tag{2}$$

where k is a function of both the temperature T and the activation energy E and follows the Arrhenius law [29]:

$$k = A \exp\left(-\frac{E}{RT}\right), \tag{3}$$

with $R = 8.314462\ \mathrm{J{\cdot}K^{-1}{\cdot}mol^{-1}}$, the ideal gas constant and A is the pre-exponential factor of the Arrhenius law. Integrations of both sides of the differential equation (Equation (2)) for annealing at temperature T_i between times t_i and t_{i+1} can be written as:

$$\int_{h_i^{Ox}}^{h_{i+1}^{Ox}} \frac{dh^{Ox}}{f(h^{Ox})} = k(T_i, E). \int_{t_i}^{t_{i+1}} g(t)dt. \quad (4)$$

We use the same model for the evolution of Copper thickness, but with decreasing values (i.e., with opposite sign before k in Equation (4)).

3.1. The Right Hand of Equation (4)

For power laws in time t: $g(t) = t^{n_{t_i}}$, the solution of the right hand of Equation (4) depends on the value of n_{t_i}.

- For $n_{t_i} = -1$, the solution involves logarithm of time:

$$\int_{t_i}^{t_{i+1}} g(t)dt = \ln(t_{i+1}) - \ln(t_i). \quad (5)$$

  The logarithmic solution is not defined for $t = 0$ and does not verify the invariance by time translation.
- For $n_{t_i} \neq -1$:

$$\int_{t_i}^{t_{i+1}} g(t)dt = \frac{(t_{i+1})^{n_{t_i}+1} - (t_i)^{n_{t_i}+1}}{n_{t_i}+1}. \quad (6)$$

3.2. The Left Hand of Equation (4)

For power laws in thickness h: $f(h^{Ox}) = (h^{Ox})^{n_{h_i}}$, the solution of the left hand of Equation (4) depends on the value of n_{h_i}.

- For $n_{h_i} = 1$, the solution involves logarithm of thickness:

$$\ln(h_{i+1}^{Ox}) = \ln(h_i^{Ox}) + k(T_i, E) \int_{t_i}^{t_{i+1}} g(t)dt. \quad (7)$$

  The logarithmic solution is not defined if copper is not oxidized. Indeed, it does not verify the boundary conditions.
- For $n_{h_i} \neq 1$, the solutions of the kinetic differential equation (Equation (2)) is:

$$(h_{i+1}^{Ox})^{1-n_{h_i}} = (h_i^{Ox})^{1-n_{h_i}} + (1-n_{h_i})k(T_i, E) \int_{t_i}^{t_{i+1}} g(t)dt. \quad (8)$$

3.3. Combination of Solutions

The laws of oxidation found in literature involve integer values of n_{hi} and n_{ti}.

- For $n_{t_i} = -1$, we obtain the logarithmic oxidation (Log) and the inverse logarithmic laws (Ilg), respectively.
  - $n_{h_i} = 0$:

$$h_{i+1}^{Ox} = h_i^{Ox} + k(T_i, E)\,(\ln(t_{i+1}) - \ln(t_i)). \quad (9)$$

    This solution of the kinetic equation has been related to a physical model by Cabrera and Mott [24]. The underlying phenomenon is the contact potential difference between the metal and the adsorbed oxygen layer. The ion diffusion is governed by the electric field produced by adsorbed oxygen on the oxide surface and the metal surface. If $f(h^{Ox})$ is an exponential function, the condition of validity of this formula is achieved if $h^{Ox} << h_r$, where h_r is a reference thickness that can be deduced from the contact potential difference (h_r being typically 10 nm–100 nm) [24]. The logarithmic oxidation law is therefore only valid for thin oxide layers, at the beginning of the oxidation process. Uhlig underlined that this oxidation law can be applied to oxide films greater than 4 nm [22]. Kusano et al. found that activation energies are 35.9, 33.9, and 33.4 kJ mol^{-1} for Cu(100),

Cu(110) and Cu(111), respectively (logarithmic oxidation law, oxide thicknesses below 5 nm) [30]. For oxide thickness between 2 nm and 4–5 nm, the tunneling effect of ions, was dominant and therefore, the logarithmic law was found [29].

- $n_{h_i} = 2$:

$$\frac{1}{h_{i+1}^{Ox}} = \frac{1}{h_i^{Ox}} - k(T_i, E)\,(\ln(t_{i+1}) - \ln(t_i)). \tag{10}$$

Mott and Cabrera showed that for thin film, the migration velocity is proportional to an exponential power of the field strength and the rate of escape of metal ions into the oxide becomes controlling. The oxidation is governed by a strong electric field due to contact potential difference between metal and adsorbed oxygen, which enables the metal ions to move through the oxide layer [24]. In this case, the inverse logarithmic equation is obtained [22,29]. The inverse logarithmic rate is actually an approximation that is not an asymptotic solution of the rate equation [29] but was found experimentally for copper [31].

- For $n_{t_i} = 0$, power laws are obtained.
  - $n_{h_i} = -3$, the quartic oxidation law (Qua) is obtained:

$$(h_{i+1}^{Ox})^4 = (h_i^{Ox})^4 + 4k(T_i, E)\,(t_{i+1} - t_i). \tag{11}$$

  - $n_{h_i} = -2$:

$$(h_{i+1}^{Ox})^3 = (h_i^{Ox})^3 + 3k(T_i, E)\,(t_{i+1} - t_i). \tag{12}$$

The cubic law (Cub) is based on the Coulomb formula that is proportional to $1/h^{Ox}$ [24]. Therefore, the diffusion of ions through the oxide film is dominant. Uhlig derived the cubic law from the density of negative charge in the oxide layer fall off. The cubic law was found to fit the experimental data, after a short growth following a logarithmic law [31]. In that reference, the activation energy for copper oxidation was 116 kJ mol^{-1}. For oxide thicknesses between 5 nm and 25 nm (cubic oxidation law), the activation energies are 95.1, 91.1, and 89.6 kJ mol^{-1} for Cu(100), Cu(110) and Cu(111), respectively [30].

  - $n_{h_i} = -1$:

$$(h_{i+1}^{Ox})^2 = (h_i^{Ox})^2 + 2k(T_i, E)\,(t_{i+1} - t_i). \tag{13}$$

The parabolic law (Par) was introduced by Wagner [23] assuming that the oxidation of metals was governed by the diffusion of ions and migration of electrons. This model cannot be applied at low temperature of annealing (T < 700 K) [1]. Cabrera and Mott stated that this law is valid for sufficiently high temperature and sufficiently thick film [24]. In this case, Copper or oxygen diffuses through the oxide layer under a concentration gradient which is proportional to $1/h$. Ramirez et al. found a good agreement between experiments and the parabolic oxidation law for oxide thicknesses beyond 10 nm [32]. In this case, they obtained an activation energy of 33.1 kJ mol^{-1}. For oxide thickness less than about 2 nm, the tunneling effect of electrons, was dominant and therefore, the parabolic law was found [29].

  - $n_{h_i} = 0$:

$$(h_{i+1}^{Ox}) = (h_i^{Ox}) + k(T_i, E)\,(t_{i+1} - t_i). \tag{14}$$

For copper films about 50 nm thickness, Rauh et Wißmann found that linear oxidation law (Lin) was a suitable one, even if they observed a tendency towards parabolic behavior [33]. They explained this oxidation law by a competition between the interface reaction and the volume diffusion.

Despite physical background of the models, the resulting solutions are typically fitting functions, as some of them verify neither the invariance by time translation nor the boundary condition ($h^{Ox}(t = 0) = 0$). Moreover, some of them do not verify the necessary condition of dimensional homogeneity [34] (the argument of logarithm functions is not dimensionless [1]).

In the following, we consider that integer or non integer values of n_{h_i} and n_{ti} are possible for the fitting of experimental data without any a priori assumption on the oxidation law. Therefore, we propose two approaches to solve the inverse problem in order to recover the activation energy (and therefore the possible oxidation law). The method is applied to three samples that are successively annealed.

4. Materials: Copper Oxidation of the Same Sample

Three samples of respective target thicknesses $tt = 10$ nm, $tt = 30$ nm and $tt = 50$ nm of Copper deposition are successively annealed at temperatures T. Appendix B gives details on the sample preparation and on the measurement of initial and final thicknesses of copper and oxide by Scanning Electron Microscopy, Multi Angle Incident spectroscopy, Atomic Force Microscopy, Spectroscopic Ellipsometry and UV-Visible Spectroscopy. The intermediate thicknesses are not measured to avoid possible destruction of the samples. Figure 1 gives an overview of the annealing process for each investigated sample [8].

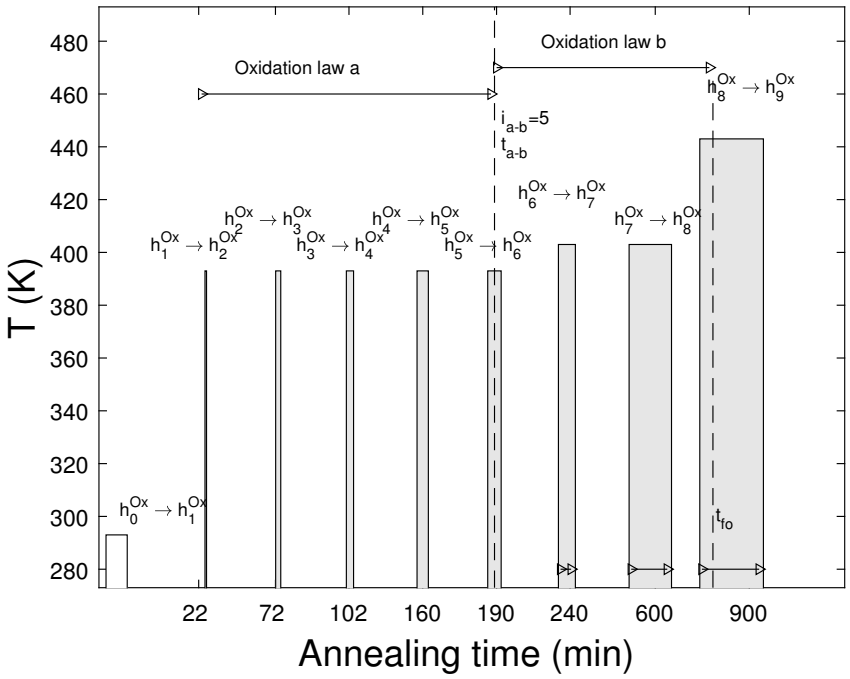

Figure 1. Annealing temperature T_i (K) as a function of annealing time t_i (min). The annealing time is indicated above each pattern. The thickness of each sample at the beginning and at the end of the annealing process are h_i^{Ox} and h_{i+1}^{Ox}, respectively. The initial white rectangle on the left corresponds to the fabrication of the initial sample. The initial and the final thicknesses of oxide (after 8 successive annealing) are measured: $m(h_1)$ and $m(h_9)$ (see Appendix B). The full oxidation t_{fo} may occur before t_9 ($t_{fo} \in [0; t_9]$).

We consider $h_1^{Ox} = h(0)$ and $h_9^{Ox} = h^{Ox}(t_{fo})$ that are the initial (before annealing) and the final oxide thicknesses (Copper is fully oxidized). These values are measured and subject to uncertainty (Table A1 of Appendix B). Full oxidation of copper occurs at $t_{fo} \leq t_9$ ($h^{Cu} = 0$ for $t \in [t_{fo}; t_9]$). For any oxidation law with the Arrhenius model (Equation (3)), and for a given value of h_1^{Ox}, randomly chosen within the intervals of uncertainties of measurement (Appendix B), we evaluate numerically the successive intermediate thicknesses $h_{2..9}^{Ox}$ (Equation (8)). If h_9^{Ox} lays within the interval of uncertainty of $m\left(h_9^{Ox}\right)$ (Table A1 in

Appendix B), then the oxidation law is considered as a solution of the inverse problem. The fitness function F (Equation (1)) is written with $h_{end} = h_9$. To avoid artificial attraction toward the middle of uncertainty intervals, the value of the fitness function is set to zero if the calculated thickness of copper and oxide lays in the interval of uncertainty of their measurement.

We propose to investigate the classical laws (with integer powers of thickness and time): linear, parabolic, cubic, logarithmic and inverse logarithmic laws in a first approach. Then we will suppose two successive laws. Finally, we will fit the data with non integer powers (two and three laws of oxidation). The domain of search are: $[0; 200]$ for prefactors (A), $[0; t_9]$ for the time of complete oxidation t_{fo} and $[0; 200]$ kJ mol^{-1} for the activation energies (E).

5. Results and Discussion

The resolution of the inverse problem consists in retrieving unknowns parameters of the model from experimental data (the measured initial and final thicknesses of copper and oxide). In our case, the unknown parameters are the copper and oxide thicknesses for each annealing step, the activation energy, the prefactor in the Arrhenius law (Equation (3)), the oxidation laws, and the time at which the complete copper oxidation takes place. The activation energy may depend on the oxide thickness, therefore, we propose four studies, by increasing the degrees of freedom of the problem as following:

- In Section 5.1, we calculate the unknown parameters by considering a single oxidation law for all annealing steps. In this case, the classical oxidation laws are tested systematically (the powers in the oxidation law are integers).
- In Section 5.2, two oxidation laws are used and the time at which the change of oxidation law occurs, is calculated.
- In Section 5.3, two oxidation laws are used and the time at which the change of oxidation law occurs, as well as the powers in the oxidation laws, are computed. In this case, the degree of freedom is increased as we no more consider only the classical laws.
- In Section 5.4, three successive oxidation laws are considered, and the two time values at which the oxidation laws change, are retrieved as well as the powers in the oxidation laws.

5.1. Fit of Data with a Single Classical Law (Integer Powers)

If we suppose that the same physical phenomenon governs the whole oxidation process, for all annealings of the same sample, a single oxidation law is used to fit the data. Therefore, the unknowns of the problem are the powers n_h and n_t in the tested solution of the kinetic differential equation (Equation (8)), the time of complete oxidation t_{fo} that occurs before the end of the last annealing, the activation energy E and the prefactor A (Equation (3)). The 1000 realizations of the algorithm give a sample of acceptable results, using random initial thicknesses in the interval of uncertainty of their measurement. Therefore, the relative frequency P of occurrence can be calculated and the most probable solutions can be deduced.

We also evaluate the activation energy (E_{LR}) obtained from the classical method, that consists in calculating the slope of the logarithm of oxidation rate as a function of $1/T$, by using linear regression. For the classical method, it is necessary to achieve the measurement of the intermediate thicknesses and their uncertainties (given in [8]). To take into account these uncertainties, we use the method described in Appendix C. That contrasts with the new proposed method which only necessitate the measurement of the initial and final thicknesses (the intermediate ones are numerically evaluated).

Table 1 gives the results and Figure 2 illustrates the activation energies found for the three samples. The results from both the classical method (E_{LR}) and the new method (E) can be compared.

Table 1. For each sample of initial target thickness of copper deposition tt, the recovered laws and corresponding parameters: the activation energy E (kJ mol^{-1}) and prefactor A in the Arrhenius law, final time of oxidation t_{fo} (min) by decreasing relative frequency P. The values (.) are the standard deviation of the mean value. The activation energy E_{LR} and uncertainties retrieved from classical method (linear regression of the oxidation rate as a function of the inverse of temperature $1/T$ (see Appendix C). The values (.) are the uncertainties on E_{LR} (see Appendix C).

Law		Sample S1 (tt = 10 nm) Parameters	Sample S2 (tt = 30 nm) Parameters	Sample S3 (tt = 50 nm) Parameters
Lin	E	46.8 (3.8)	42.7 (3.9)	41.2 (3.4)
	A	103 (2)	99 (2)	99 (2)
	t_{fo}	456 (8)	459 (8)	457 (8)
	P	0.31	0.40	0.44
	E_{LR}	20 (26)	15 (29)	14 (27)
Log	E	21.2 (3.1)	17.4 (2.9)	15.7 (2.8)
	A	102 (2)	102 (2)	99 (2)
	t_{fo}	443 (8)	448 (8)	451 (8)
	P	0.31	0.40	0.44
	E_{LR}	18.2 (4.5)	14.5 (4.2)	12.8 (4.2)
Par	E	40.4 (3.5)	32.6 (2.8)	29.5 (2.4)
	A	94 (2)	86 (2)	87 (3)
	t_{fo}	458 (8)	408 (11)	406 (14)
	P	0.29	0.19	0.11
	E_{LR}	13 (27)	2 (26)	0 (26)

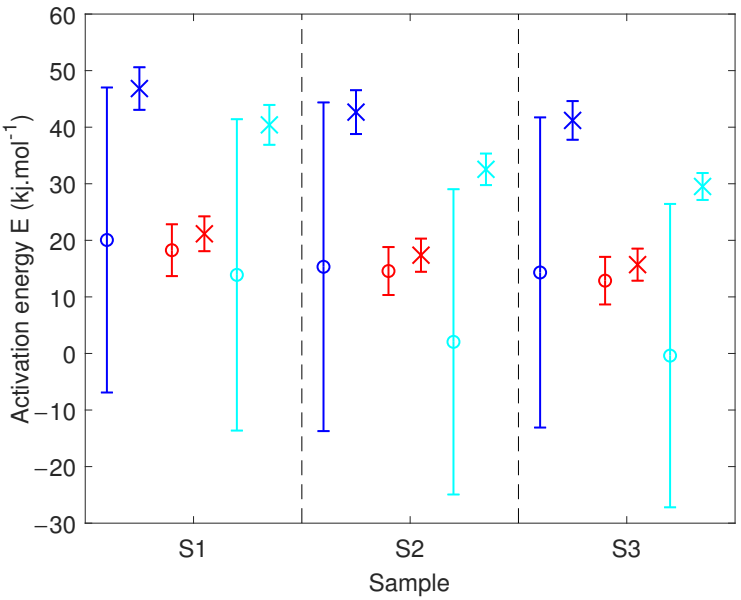

Figure 2. Activation energies (kJ mol^{-1}) and their uncertainties (error bars) retrieved from our method (x) and from classical method (o) for the three samples S1, S2 and S3 and the three oxidation laws: Lin (blue), Log (red) and Par (cyan).

For the first sample (the initial thickness of copper deposition is $tt = 10$ nm), about equal probabilities are found for the linear, the logarithmic and the parabolic oxidation laws. For the second and third samples ($tt = 30$ nm and $tt = 50$ nm, respectively), similar probabilities occur only for the linear and logarithmic oxidation laws. The other retrieved parameters are of the same order of magnitude for the three samples and for the three

oxidation laws, respectively. The values of the activation energies obtained from the classical method (E_{LR}) are smaller than those obtained from our method (E). The mean value of the activation energy calculated with our method is in the interval of uncertainties of the classical method. The uncertainty on E_{LR} is about 10 times that of our method (see Figure 2 and Table 1). Therefore, our method appears to be more efficient than the classical one.

The calculated activation energies deserve to be compared to those obtained by other authors. Depending on the conditions of Copper deposition, the pressure, the oxide thickness and the structure of oxide (defects, crystalline phase...), the value of the activation energy was found in the range [14; 126] kJ mol^{-1} [1,22,24,32,35–38]. The value of activation energy for linear and logarithmic oxidation law are in agreement with that found from the model of dominant surface reaction. A recent paper [36] has revisited the copper oxidation law in Air at low temperatures ($T < 373$ K). The oxidation rate was measured by isothermal thermogravimetric analysis and quartz crystal balance. The oxidation law was found to be logarithmic after a short linear oxidation rate. The activation energy $E = 15.9 \pm 2.5$ kJ mol^{-1} is close to ours for this oxidation law. Kusano et al. [30] found $E = 35.9$, 33.9 and 33.4 kJ mol^{-1} for Cu(100), Cu(110) and Cu(111) respectively. These values are close to those obtained for the parabolic law. In this case, the main physical phenomenons underlying the copper oxidation are the diffusion of Cu through a bulk material and the copper grain boundary diffusion in copper oxide.

Let us underline that the measurement of intermediate thicknesses is not required for our method (only the measurements of the initial and final thicknesses are necessary, with their uncertainties). That contrasts with the classical method for which all the intermediate thicknesses must be measured at the end of each annealing step.

Nevertheless, if only one oxidation law is considered, the equal probability of the possible laws does not allow to conclude on the law governing the oxidation. This suggests that a single law is not sufficient to describe the whole oxidation process. Moreover, Kusano et al., demonstrated that the oxidation law, and therefore the activation energy, depend on the thickness of oxide: the logarithmic law was obtained for oxide thickness under 5 nm, cubic behavior in the range 5–25 nm ($E \in [33.4; 35.9]$ kJ mol^{-1}) and parabolic behavior over 25 nm ($E \in [89.6; 95.1]$ kJ mol^{-1}). In the following, we assume two successive oxidation laws as an alternative, the physical phenomenon governing the oxidation at the beginning of annealing being different from the further ones [1].

5.2. Fit of Data with Two Successive Classical Laws (Integer Powers)

Let us consider successive annealing of the same copper sample. According to the results in the above mentioned reference [1], we suppose that two successive oxidation laws a and b are possible, when the oxide thickness increases. The annealing for which the oxidation law changes is denoted i_{a-b}. In this case, the unknowns in the model are the powers (n_{ha}, n_{hb}) in the solution of the kinetic differential equations (Equation (8)), the time of complete oxidation t_{fo} that occurs before the end of the last annealing, the activation energies (E_a, E_b) and the prefactors (A_a, A_b) (Equation (3)).

Two successive laws of oxidation (the oxidation law changes at annealing step i_{a-b}) are considered without any a priori hypothesis on the physical phenomenon. Therefore, we test all the oxidations laws retrieved from literature. The domain of search is $\{-3; \ldots; +3\}$ for the integer powers of thickness in oxidation law (n_{ha}, n_{hb}) and $\{-1; 0\}$ for both powers of time (n_{ta}, n_{tb}) (see Section 3). We test all combinations of the laws of the first oxidation and the second law (6×6 cases), for any i_{a-b}, from 1000 random draw of the first thicknesses of copper and oxide, in their interval of uncertainties. The result is acceptable if the fitness function F (Equation (1)) is equal to 0. Table 2 gives the most probable oxidation laws with the mean values and the standard deviation of the mean of each unknown values.

The probability P is about the same for the four solutions of each sample ($P \approx 0.18 - 0.25$). Among the 36 combinations of the 6 oxidation laws (Log, Ilg, Qua, Cub, Par, Lin), only logarithmic and linear ones are the most probable oxidation laws. The index i_{a-b} of

the change of law corresponds to the fourth or fifth annealing. Consequently, we may conclude that the first oxidations obey to a different phenomenon from that for the further annealings. Nevertheless, the probabilities do not able to choose between the linear and the logarithmic oxidation laws, in the two zones. For each couple of oxidation laws, the activation energies varies roughly from 58 to 81 kJ mol^{-1} for the first oxidation law and from 56 to 81 for the second one. Even if these values are close to those found in Refs. [1,15,30,37,38], the uncertainties on the measurement of thickness produce equivalent solutions in terms of probabilities. The consequence is that the activation energies cannot be deduced. The possible reason of the dispersion activation energies is that the oxidation cannot be attributed to a single phenomenon. Therefore, the search of non integer powers in the solutions of the kinetic equation in Section 3 could be an alternative.

Table 2. For each sample of initial target thickness of copper deposition tt, the recovered laws and corresponding parameters: activation energies (E_a, E_b) (kJ mol^{-1}) and prefactors (A_a, A_b), index of the annealing for which the oxidation law changes (i_{a-b}), the time of full oxidation t_{fo} (min) and the relative frequency of occurrence of the solution, P. We only indicate the values of P that are greater than 0.1 and we sort solutions by decreasing values of P. The values $(.)$ are the standard deviation of the mean value.

	Sample S1 (tt = 10 nm)		**Sample S2 (tt = 30 nm)**		**Sample S3 (tt = 50 nm)**	
	Law	**Parameters**	**Law**	**Parameters**	**Law**	**Parameters**
E_a	Lin	80.79 (0.68)	Lin	71.84 (0.68)	Lin	68.23 (0.66)
A_a		101.87 (0.73)		99.80 (0.71)		101.42 (0.70)
i_{a-b}		4.50 (0.02)		4.50 (0.02)		4.50 (0.02)
E_b	Lin	80.35 (0.61)	Log	64.77 (0.77)	Log	64.31 (0.77)
A_b		101.85 (0.73)		100.32 (0.71)		99.20 (0.70)
t_{fo}		457.0 (3.3)		451.9 (3.2)		451.4 (3.2)
P		0.18		0.24		0.25
E_a	Lin	74.72 (0.66)	Lin	78.60 (0.70)	Lin	76.71 (0.69)
A_a		100.65 (0.73)		98.99 (0.72)		98.82 (0.71)
i_{a-b}		4.50 (0.02)		4.50 (0.02)		4.50 (0.02)
E_b	Log	67.09 (0.75)	Lin	77.72 (0.63)	Lin	74.52 (0.62)
A_b		101.11 (0.74)		100.95 (0.72)		100.14 (0.70)
t_{fo}		455.5 (3.3)		450.7 (3.2)		448.8 (3.2)
P		0.18		0.24		0.25
E_a	Log	70.95 (0.78)	Log	69.61 (0.80)	Log	69.13 (0.79)
A_a		102.32 (0.73)		100.00 (0.70)		100.55 (0.69)
i_{a-b}		4.50 (0.02)		4.50 (0.02)		4.50 (0.02)
E_b	Lin	77.40 (0.60)	Lin	72.48 (0.60)	Lin	70.25 (0.60)
A_b		101.50 (0.74)		101.11 (0.72)		100.31 (0.69)
t_{fo}		458.3 (3.3)		454.8 (3.2)		457.0 (3.1)
P		0.18		0.18		0.18
E_a	Log	64.84 (0.77)	Log	60.13 (0.77)	Log	59.40 (0.76)
A_a		101.13 (0.73)		100.58 (0.71)		101.04 (0.70)
i_{a-b}		4.50 (0.02)		4.50 (0.02)		4.50 (0.02)
E_b	Log	63.59 (0.75)	Log	61.01 (0.76)	Log	57.01 (0.74)
A_b		101.02 (0.73)		99.88 (0.72)		101.25 (0.69)
t_{fo}		459.1 (3.3)		448.5 (3.2)		450.7 (3.2)
P		0.18		0.18		0.18

5.3. Fit of Data with Two Successive Laws (Non Integer Powers)

The domain of search are $[-3;+3]$ for the non integer powers of thickness in oxidation law (n_{ha}, n_{hb}), and $[-1;+1]$ for the powers of time (n_{ta}, n_{tb}). Thousand realizations of the same algorithm are achieved with initial random draw of the initial thicknesses of copper and oxide in their uncertainty intervals of measurement. Table 3 shows the mean values and the standard deviation of the unknowns of the model.

Table 3. For each sample of initial target thickness of copper deposition tt, the corresponding parameters: mean value E and standard deviation of the mean value $(.)$ of the first and second retrieved activation energies (kJ mol^{-1}), power n_h of thicknesses, prefactor A of both oxidation laws, i_{a-b} index of sample for which the oxidation law changes, final time of oxidation t_{fo} (min), over 1000 realizations of algorithm for each i_{a-b} from 2 to 8. The target thicknesses of Copper deposition for each investigated sample. The index of the change annealing for which the oxidation law changes is i_{a-b}. For $i < i_{a-b}$ the first oxidation law is valid, with E_a as activation energy. For $i \geq i_{a-b}$ the second oxidation law takes over, with activation energy E_b.

	Sample S1 (tt = 10 nm)	**Sample S2 (tt = 30 nm)**	**Sample S3 (tt = 50 nm)**
E_a	95.4 (1.5)	101.4 (1.6)	101.6 (1.7)
A_a	99.6 (1.6)	101.6 (1.6)	98.3 (1.7)
n_{ha}	0.05 (0.04)	−0.00 (0.04)	0.12 (0.05)
n_{ta}	−0.51 (0.01)	−0.50 (0.01)	−0.51 (0.01)
i_{a-b}	2 (0)	2 (0)	2 (0)
E_b	55.1 (0.7)	45.8 (0.3)	44.6 (0.3)
A_b	101.4 (1.5)	98.5 (1.7)	100.8 (1.7)
n_{hb}	0.31 (0.01)	0.23 (0.01)	0.24 (0.01)
n_{tb}	−0.49 (0.01)	−0.50 (0.01)	−0.50 (0.01)
t_{fo}	449 (7)	457 (7)	460 (8)

The results show that two successive oxidation laws can describe the successive annealing of each of these three investigated samples. The activation energy of the first oxidation law is in $[99.8;103.3]$ kJ mol^{-1} for samples S2 and S3 and in $[93.9;96.9]$ kJ mol^{-1} for sample S1. The activation energy E_a is close to that found by Cabrera and Mott theory of cation diffusion by electrostatic field [24] (107 kJ mol^{-1}, and that in Ref. [30]. These results are in agreement with those by Piippo et al. [39] and Fujita et al. [1] (grain boundary diffusion). The annealing step for which the oxidation law changes is the same for the three samples ($i_{a-b} = 2$). The time of final oxidation is also about the same for the three samples ($t_{fo} \in [442;468]$ min). The activation energy of the second oxidation law is in $[44.3;55.8]$ kJ mol^{-1}: 50.5 kJ mol^{-1} was found by [1,39] (surface reaction step). The full oxidation time increases with the initial sample thickness. The time of final oxidation also is about the same (from 440 to 470 min). These results suggest that the method is robust.

The powers of time n_t are close to -0.5 for the two laws for the three samples S1, S2 and S3. These results suggest that both polynomial and logarithmic laws are underlying oxidation. For the first law of oxidation, the oxidation can be linear or logarithmic. For the second law, the oxidation law may be logarithmic or inverse logarithmic. This result is in agreement with those obtained assuming a single law obtained for thin films [30].

To select the oxidation laws that preserve the invariance by time translation, we also apply the method with $n_{ta} = n_{tb} = 0$, and the obtained results are shown in Table 4.

For the three samples, the prefactors are about 100, i_{a-b} is equal to 2 or 3 and t_{fo} lays between 434 and 457 min. The values of n_{ha} and n_{hb} are between 0 and 1, that suggests laws that differ from the classical ones. We found about the same activation energy E_a (Tables 3 and 4) as in Ref. [1,38] (99.3 kJ mol^{-1}, 80 kJ mol^{-1} respectively). Such value is compatible with the Cu diffusion through the bulk oxide. At our temperature conditions, the oxidation was found to follow a logarithmic oxidation law that might be governed by

the formation of CuO nuclei in the Cu2O host. The second activation energy, obtained for thicker oxide layers, is about 52.7–56.7 kJ mol^{-1}. These values are corresponding to the surface oxidation step in Ref. [37].

Table 4. For each sample of initial target thickness of copper deposition tt, the corresponding parameters: mean value E and standard deviation of the mean value $(.)$ of the first and second retrieved activation energies (kJ mol^{-1}), power n_h of thicknesses, prefactor A of both oxidation laws, i_{a-b} index of sample for which the oxidation law changes, final time of oxidation t_{fo} (min), over 1000 realizations of algorithm for each i_{a-b} from 1 to 8. The target thicknesses of Copper deposition for each investigated sample. The index of oxidation law change is i_{a-b}. For $i < i_{a-b}$ the first oxidation law is valid, with E_a as activation energy. For $i \geq i_{a-b}$ the second oxidation law takes over, with activation energy E_b. The solutions verify the invariance by time translation $(n_{ta} = n_{tb} = 0)$.

	Sample S1 (tt = 10 nm)	**Sample S2 (tt = 30 nm)**	**Sample S3 (tt = 50 nm)**
E_a	95.5 (1.3)	99.2 (1.3)	99.1 (1.4)
A_a	100.4 (1.4)	101.1 (1.4)	99.4 (1.4)
n_{ha}	0.23 (0.04)	0.24 (0.04)	0.24 (0.04)
i_{a-b}	3 (0)	3 (0)	2 (0)
E_b	55.7 (0.6)	56.0 (0.7)	53.3 (0.6)
A_b	99.9 (1.4)	100.7 (1.4)	101.7 (1.4)
n_{hb}	0.57 (0.01)	0.82 (0.01)	0.84 (0.01)
t_{fo}	440 (6)	451 (6)	442 (6)

As a conclusion, the search of non integer powers in the solutions of the kinetic equation appears to be efficient. The linear oxidation law appears to be dominant for the first oxidations. However, these intermediate values of n_h lead us to test the method for three successive laws of oxidation [29,30].

5.4. Fit of Data with Three Successive Laws (Non Integer Powers)

For each sample of initial target thickness of copper deposition $tt = 10, 30, 50$ nm, we retrieve the parameters of three successive laws of oxidation (Table 5).

The activation energy E_a is between 105.8 and 108.8 kJ mol^{-1}. The recovering of intervals of uncertainties suggests that a single activation energy around 105.8–108.8 kJ mol^{-1} is characteristic of this first oxidation step, that is little bit greater than E_a found with two laws (Tables 3 and 4), but close to the value in Ref. [24] (Coulomb energy for moving oxide to the surface) and given in Ref. [1] for grain boundary diffusion. For annealing from $i_{a-b} = 2$ to $i_{b-c} = 5$, the activation energy E_b is between 76.7 and 86.9 kJ mol^{-1}. In Ref. [29], the activation energy was found about 79–88 kJ mol^{-1}. The third activation energy $E_c \approx 47.6 - -58.5$ kJ mol^{-1}. By comparing the present results obtained from three successive laws of oxidation to those resulting from only two, we observe that the numerical values of the two activation energies given in the previous section (94.2–100.5 and 52.7–56.7 kJ mol^{-1}) are intermediate between the three ones obtained here.

The activation energy decreases as the oxide thickness is growing. This behavior could be related to the grain structure of thick oxide, that may increase the possible migration of oxygen through it. The decrease of the activation energy with increasing thickness of oxide has been attributed to the granular structure of oxide. In this case, Lawless stated that the material transport is no longer rate limiting. The phase boundary control leads to linear oxidation law [29]. In Ref. [1], the grain boundary diffusion of Copper ions in oxide explain activation energies of about 100 kJ mol^{-1}. Moreover, the values we find for n_h are close to 0, between -1 and 0, and -2 and -1, for the three successive oxidation laws. These results may explain that parabolic and cubic laws have been found in Ref. [1], by using the classical method of linear regression.

Table 5. For each sample of initial target thickness of copper deposition tt, the corresponding parameters: mean value E and standard deviation of the mean value $(.)$ of the first and second retrieved activation energies (kJ mol^{-1}), power n_h of thicknesses, prefactor A of the three oxidation laws, i_{a-b} and i_{b-c} indexes of annealing for which the oxidation law changes (and time of change: t_{a-b} and t_{b-c}), final time of oxidation t_{fo} (min), over 1000 realizations of algorithm for each i_{a-b} and i_{b-c} from 2 to 8. The target thicknesses of Copper deposition for each investigated sample. The solutions verify the invariance by time translation $(n_{ta} = n_{tb} = 0)$.

	Sample S1 (tt = 10 nm)	**Sample S2 (tt = 30 nm)**	**Sample S3 (tt = 50 nm)**
E_a	108.0 (0.8)	108.0 (0.7)	106.5 (0.7)
A_a	103.0 (0.9)	103.3 (0.8)	103.2 (0.7)
n_{ha}	0.11 (0.03)	0.24 (0.02)	0.29 (0.02)
i_{a-b}	2 (0)	2 (0)	2 (0)
t_{a-b}	33 (1)	35 (1)	37 (1)
E_b	86.1 (0.8)	80.5 (0.8)	77.3 (0.7)
A_b	104.0 (0.9)	105.9 (0.8)	103.5 (0.7)
n_{hb}	−0.36 (0.03)	−0.28 (0.02)	−0.28 (0.02)
i_{b-c}	5 (0)	5 (0)	5 (0)
t_{b-c}	182 (3)	185 (3)	183 (2)
E_c	57.7 (0.8)	49.7 (0.8)	48.3 (0.7)
A_c	103.6 (0.9)	105.3 (0.8)	106.6 (0.7)
n_{hc}	−1.82 (0.01)	−1.68 (0.01)	−1.54 (0.01)
t_{fo}	478 (4)	480 (4)	481 (3)

Figure 3 show the evolution of the retrieved copper and oxide thicknesses as a function of time. The decreasing of copper thicknesses are counterbalanced by the increase of oxide one. The final oxide thickness are 1.7, 1.9 and 1.7 times the initial copper ones, for samples S1, S2 and S3, respectively. These ratios are of the same order as the spatial expansion of crystalline oxide relatively to copper: 1.68–1.77 [21].

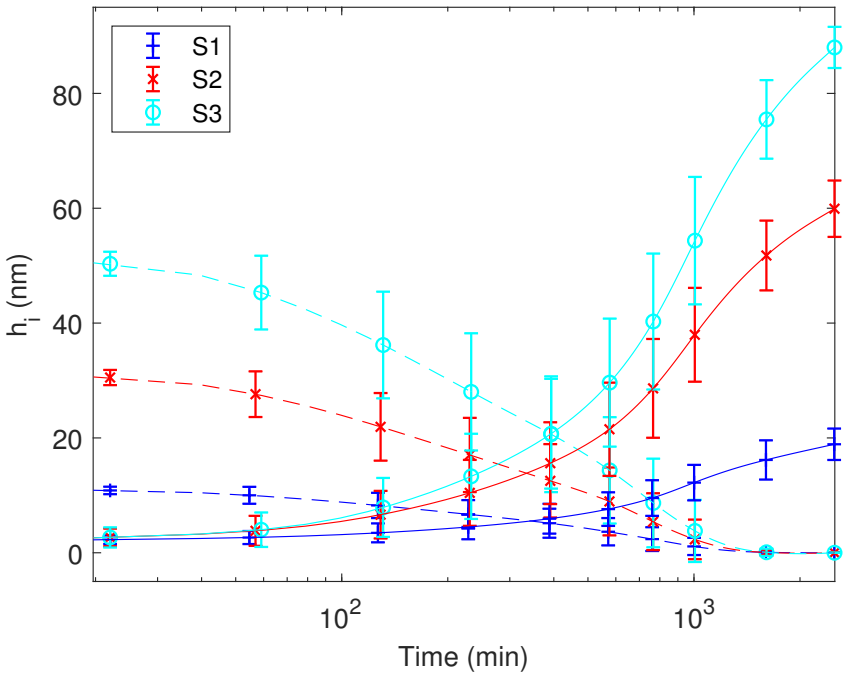

Figure 3. Retrieved Copper (dashed line) and oxide (solid line) thicknesses and their uncertainties as a function of time (logarithmic scale) for the three samples S1, S2 and S3.

Only the initial and final thicknesses are measured by Scanning Electron Microscopy, Multi Angle Incident spectroscopy, Atomic Force Microscopy, Spectroscopic Ellipsometry (see Appendix B). To assess our method, we compare the retrieved intermediate oxide thicknesses with those obtained from two different indirect measurement techniques (UV-visible spectroscopy) that are not destructive (see Ref. [6], 9 measured oxide thicknesses for each sample and [8], 6 data for each sample). Moreover, we verified that the ratio of oxide to copper thickness corresponds well with the theoretical values given by crystallography. Figures 4–6 show the three data sets for each of the three substrates (S1, S2 and S3) respectively.

For the sample S1, at each oxidation time, we observe the overlap of the uncertainties intervals (Figure 4). Therefore, the retrieved intermediate oxide thickness we found are in agreement with the indirect measurements in Refs. [6,8]. The ratio of the last oxide thickness to the copper initial one is in $[1.1; 2.5]$ in coherence with the theoretical spatial expansion of crystalline oxide relatively to copper (i.e., in $[1.68; 1.77]$ [21]).

For the sample S2, our results are in agreement with those in Ref. [6] for the corresponding oxidation times (Figure 5). Only the two last intervals of uncertainties are not overlapping with those of the measurements in Ref. [8]. However, the ratio of the final oxide thickness to the copper initial thickness (between 1.4 and 2.3) is closer to the theoretical spatial expansion of crystalline oxide relatively to copper (between 1.68 and 1.77) than that calculated from data in Ref. [8] (between 0.3 and 1.1).

For each oxidation step of sample S3, the intervals of uncertainties are overlapping (Figure 6). Moreover, the ratio of the last oxide thickness to the copper initial one is between 1.44 and 1.89. The theoretical spatial expansion of crystalline oxide relatively to copper being between 1.68–1.77 [21], we can conclude that the retrieved oxide thickness have physical sense.

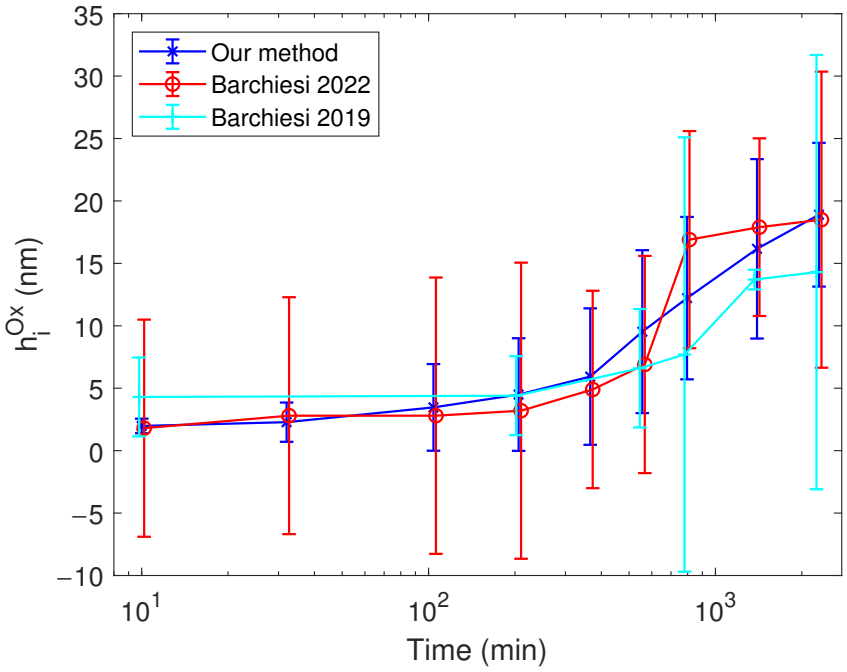

Figure 4. Oxide thicknesses obtained by our method (blue 'x'), by the method based on UV-Visible-NIR Absorbance Fitting in Ref. [6] (red 'o') and in Ref. [8] (cyan '+') as a function of time (logarithmic scale) for the sample S1. The error bars are the intervals of uncertainties (standard deviations).

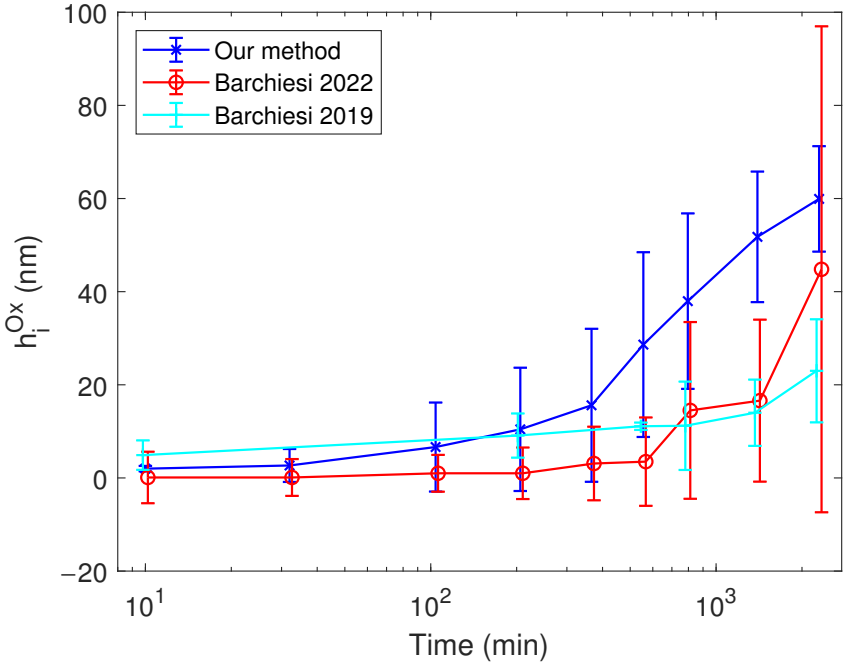

Figure 5. Oxide thicknesses obtained by our method (blue 'x'), by the method based on UV-Visible-NIR Absorbance Fitting in Ref. [6] (red 'o') and in Ref. [8] (cyan '+') as a function of time (logarithmic scale) for the sample S2. The error bars are the intervals of uncertainties (standard deviations).

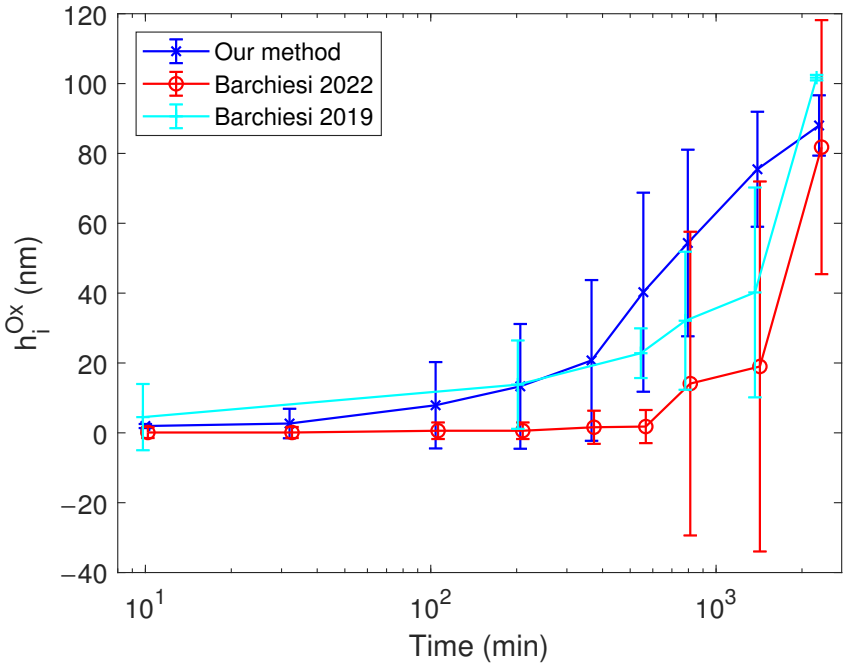

Figure 6. Oxide thicknesses obtained by our method (blue 'x'), by the method based on UV-Visible-NIR Absorbance Fitting in Ref. [6] (red 'o') and in Ref. [8] (cyan '+') as a function of time (logarithmic scale) for the sample S3. The error bars are the intervals of uncertainties (standard deviations).

For the three samples, S1, S2 and S3, we obtain oxide thicknesses that are in agreement with the measured ones in Refs. [6,8]. Moreover, our values of ratio of the final oxide thickness to the initial copper one, are in agreement with those obtained from theoretical calculations.

6. Conclusions

The proposed method for calculating the activation energy is hypothesis free about the oxidation law. The parameters of two and three successive laws of oxidation are retrieved: the activation energies, the prefactors, the functions of thicknesses and time, and the time of the end of oxidation, as well as the sample for which the oxidation law changes. The resolution of the inverse problem permits to retrieve the thicknesses of copper and oxide and their uncertainties as a function of time. The main advantages of our method are following. No a priori knowledge on the physic law (or multiple successive laws) governing the oxidation are required. Moreover, only the initial and final measurement of thicknesses are necessary. The times at which the oxidation laws change and at which the complete copper oxidation takes place, can be retrieved. We applied the method to three samples, the results are consistent between the three samples, and therefore, the method appears to be robust. We have shown that the activation energies found are in agreement with some found in the literature (about 105–109 kJ mol^{-1} for the first oxidation law; 76–87 kJ mol^{-1} for the second one, and 47–59 kJ mol^{-1} for the third one). The uncertainties on the measurement of initial and final thickness explain the dispersion of these results.

These values are coherent with those deduced from the ratio of the spatial expansion of crystalline oxide relatively to copper. Such a method is generic and could be applied to any oxidation or solid state chemical reaction (metal and metal-oxyde layer). The proposed method could also be used to improve the calculation of optical properties from spectroscopic data [6].

Author Contributions: Conceptualization, D.B.; methodology, D.B. and T.G.; software, D.B.; validation, D.B. and T.G.; writing—original draft preparation, D.B.; writing—review and editing, D.B. and T.G. All authors have read and agreed to the published version of the manuscript.

Funding: This research received no external funding.

Institutional Review Board Statement: Not applicable.

Informed Consent Statement: Not applicable.

Data Availability Statement: The original contributions presented in the study are included in the article, further inquiries can be directed to the corresponding author.

Conflicts of Interest: The authors declare no conflicts of interest.

Abbreviations

The following abbreviations are used in this manuscript:

MDPI	Multidisciplinary Digital Publishing Institute
DOAJ	Directory of open access journals
Qua	Quartic oxidation law
Cub	Cubic oxidation law
Par	Parabolic oxidation law
Lin	Linear oxidation law
Log	Logarithmic law
Ilg	Inverse logarithmic law
PSO	Particle Swarm Optimization

Appendix A. Particle Swarm Optimization (PSO) Method

PSO is an iterative algorithm which goal is to find the parameter set (D unknowns of the problem in the present case) that minimizes a fitness function F (Equation (1)). The N decision parameters set x_{j+1} (the unknowns of the problem of optimization) are moving in the bounded space of search at each iteration j according the following rule:

$$\begin{pmatrix} v_{j+1} \\ x_{j+1} \end{pmatrix} = \underbrace{\begin{pmatrix} \omega_j & -\phi_1 - \phi_2 \\ \omega_j & 1 - \phi_1 - \phi_2 \end{pmatrix}}_{M_j} \begin{pmatrix} v_j \\ x_j \end{pmatrix} + \begin{pmatrix} \phi_1.p_j + \phi_2.g_j \\ \phi_1.p_j + \phi_2.g_j \end{pmatrix}, \tag{A1}$$

where v is the translation vector of x in the space of search (also called velocity), $\phi_1 = c_1 \cdot r_1$, $\phi_2 = c_2 \cdot r_2$, c_1 and c_2 are coefficients called cognitive and social weights respectively, r_1 and r_2 are random numbers following uniform law of probability in $[0, 1]$, ω_j is the inertia weight, p_j is the best position of each particle and g_j the best one of all particles, both found along the previous iterations. If v_j and x_j are such as $x_{j+1} = x_j + v_j$ is exiting of the domain of search, x_j is randomly regenerated in the domain of search.

The determinant of M_j must be non zero: $det(M_j) \neq 0$, therefore $\omega + \phi_1 + \phi_2 \neq 0$. The matrix M_j is strictly diagonal dominant if the following relations are fulfilled:

$$\begin{cases} |\omega_j| & < & |1 - \phi_1 - \phi_2| \\ |\phi_1 + \phi_2| & < & |\omega_j| \end{cases} \Rightarrow |\phi_1 + \phi_2| < |\omega_j| < \frac{1}{2}. \tag{A2}$$

The possible update of p_j raised a rewriting of Equation (A1) including this quantity in vectors [40]. If we also consider the update of g_j, we obtain:

$$\begin{pmatrix} v_{j+1} \\ x_{j+1} \\ p_{j+1} \\ g_{j+1} \end{pmatrix} = \begin{pmatrix} \omega_j & -\phi_1 - \phi_2 & \phi_1 & \phi_2 \\ \omega_j & 1 - \phi_1 - \phi_2 & \phi_1 & \phi_2 \\ M_j^{3,1} & M_j^{3,2} & M_j^{3,3} & M_j^{3,4} \\ M_j^{4,1} & M_j^{4,2} & M_j^{4,3} & M_j^{4,4} \end{pmatrix} \cdot \begin{pmatrix} v_j \\ x_j \\ p_j \\ g_j \end{pmatrix}. \tag{A3}$$

Four cases occur depending on the possible update of p_j and g_j by x_j leading to different values of $M_j^{m,n}$. The convergence of iterative algorithm requires the spectral radius to be lower than 1, and the conditions of convergence are:

$$\Gamma = \left| \frac{\sqrt{(\omega - \alpha - 1)^2 - 4x} + \omega - \alpha + 1}{2} \right| < 1, \tag{A4}$$

where $\alpha = \phi_2$ if p_j is the only one to be updated, $\alpha = \phi_1$ if g_j is the only one to be updated, $\alpha = \phi_1 + \phi_2$ if neither p_j or g_j are updated. If both p_j and g_j are updated, the condition of convergence is $|\omega| < 1$. These four conditions must be fulfilled and are less restrictive than the diagonal dominant one. We obtain the same condition as in Ref. [40] but now for ϕ_1, ϕ_2 and $\phi_1 + \phi_2$. We summarize the spectral radius conditions of convergence:

$$|\omega_j| < 1, \tag{A5}$$

$$c_1.r_1 + c_2.r_2 < 2(1 + \omega_j). \tag{A6}$$

If we handle the convergence of x_j toward g_j at the end of the evolutionary loop, we obtain the necessary decrease of v_j toward 0. Therefore ω_j must tends toward 0 at the end of the evolutionary loop. We chose a linear decrease of ω_j as following:

$$\omega_j = 1 - j/\max(j), \tag{A7}$$

where $\max(j)$ is one of the two stop criterion of the evolutionary loop, the second one being an acceptable value of the fitness function. According to the convergence condition (Equation (A6)), c_1 and c_2 are:

$$c_1 = c_2 = 1 + \omega_j. \tag{A8}$$

Therefore, c_1 and c_2 are decreasing from 2 to 1 for $j = 1$ and $\max(j) = 300$ respectively, even if, for this choice, the condition of dominant diagonal is not verified.

The initial parameters set and velocity are randomly generated in the space of search [41], and a family of $N = 30$ parameters sets. The maximum number of iterations of the PSO loop is set to 300 to accelerate the resolution of the inverse problem. If the fitness function verifies $F = 0$, the second stop criterion is reached. At the end of the evolutionary loop, the maximum of allowed iterations is reached or the value of fitness function (Equation (1)) is smaller than 1%, the best solution is used as starting point for a gradient descent method, to try to improve the solution.

Appendix B. Experiments: Sample Elaboration and Thicknesses Measurements

Appendix B.1. Sample Elaboration

The experimental data were obtained by Deniz Cakir [21]. Three copper samples are progressively oxided under different annealing time and temperature. The target copper thickness tt of each sample S1, S2 and S3 are 10, 30 and 50 nm respectively. The samples are obtained from thermal evaporation and deposition on a glass substrate by using the following process:

- Copper rod (purity of 99.999 %, purchased from Alfa Aesar), placed 18 cm below the target substrate,
- Sublimation of the copper rod (120 A, 1 mPa), tungsten crucible, as a counter electrode,
- Fused silica substrates (optical grade, purchased from Neyco)
- Chemical cleaning in an acetone bath, with ultrasound for 5 min.
- Physical plasma cleaning (70 % O_2/30 % N_2) for 6 min.

Low annealing temperatures are chosen to produce mainly Cu_2O [14,32,42–46] at ambient pressure P = 1.013 kPa. The annealing procedure (thermal oxidation) was summarized in Table A1 in Ref. [6] and in Figure 1.The successive annealing temperatures are below 470 K and therefore pure cuprite (Cu_2O) phase is probably obtained [36,47,48]. The complete oxidation of the copper layer occurs during the last annealing. Therefore, t_9 cannot be used in calculations. However, $m(h_9)$, the last oxide thickness is used to tune the method.

The three samples are annealed height times.

Appendix B.2. Thicknesses Measurements

The initial thicknesses of copper and oxide, before annealing ($m(h_1)$) and the last ones ($m(h_9)$), after the last annealing were measured using different measuring instruments. Intermediate thicknesses are not measured. Indeed, the required cut of samples to get cross sections for Scanning Electron Microscopy and Atomic Force Microscopy measurements, are possibly destructive for the samples. The measurement instruments were: Multiple-Angle Incident ellipsometry, Spectroscopic Ellipsometry and UV-visible spectroscopy. A bi-layer Cu/Cu_2O model was chosen with refractive index of $0.94530 + \imath 2.5997$ and $3.1137 + \imath 0.2323$ respectively for Cu and Cu_2O for Multiple-Angle Incident ellipsometry and from Sopra data for Spectroscopic Ellipsometry, $\imath$ being the pure imaginary complex number. We give the interval of uncertainty for the measurement of the oxide thicknesses for each initial (before annealing) and final (fully oxidized) samples S1, S2, and S3 in Table A1 [8]. The values of measured thicknesses are strongly depending on the measurement method. Therefore, we evaluate the uncertainties to cover all the measured values from different methods [8].

Table A1. For each sample of initial target thickness tt of copper deposition, the corresponding parameters: intervals of uncertainty of the measurement of copper and oxide thicknesses for the initial samples (before annealing) and final sample (fully oxidized) from Ref. [8]. The target thicknesses of the copper deposit for each sample were: tt = 10, 30 and 50 nm for samples S1, S2 and S3 respectively.

Measured Quantity [8]	Sample S1 tt = 10 nm	Sample S2 tt = 30 nm	Sample S3 tt = 50 nm
$m(h_1^{Cu})$	[10; 12]	[31; 35]	[51; 55]
$m(h_1^{Ox})$	[0; 5]	[0; 5]	[0; 5]
$m(h_9^{Cu})$	[0; 2]	[0; 2]	[0; 2]
$m(h_9^{Ox})$	[10; 30]	[42; 82]	[74; 104]

Appendix C. Calculation of Uncertainty on the Calculation of the Activation Energy

The general expression of the activation energy as a function of the oxidation law, solution of the kinetic equation, with the Arrhenius law is:

$$E_{LR} = RT_i \left[\ln(A) + \ln\left(\frac{G(t_{i+1}) - G(t_i)}{F(h_{i+1}) - F(h_i)} \right) \right], \tag{A9}$$

where $F(h)$ and $G(t)$ are the solutions of the kinetic equation (see Section 3). These functions depend on the oxidation law. For example, with $n_h = 0$, $F(h) = h$, and $n_t = -1$, $G(t) = \ln(t)$. With $n_t = 0$, $G(t) = t$ and we obtain solutions that verify the invariance by time translation.

The classical method used to evaluate the activation energy relies on the use of the least square linear fitting of the oxidation rate as a function of the inverse of temperature $(1/T)$:

$$-R \ln\left(\frac{F(h_{i+1}) - F(h_i)}{G(t_{i+1}) - G(t_i)} \right) = E_{LR} \frac{1}{T_i} - R \ln(A). \tag{A10}$$

The slope of the line relating the first term in Equation (A10) to $1/T$ is the activation energy. A linear regression can be applied to all experimental data to retrieve the activation energy. The uncertainty on the slope found by linear regression is the combination of standard error of this coefficient $SE(E)$ and the standard deviation $\sigma(E)$ of the slope calculated using 1000 random generations of h_i and h_{i+1} in their uncertainty intervals:

$$u(E_{LR}) = \sqrt{SE^2(E_{LR}) + \sigma^2(E_{LR})}. \tag{A11}$$

References

1. Fujita, K.; Ando, D.; Uchikoshi, M.; Mimura, K.; Isshiki, M. New model for low-temperature oxidation of copper single crystal. *Appl. Surf. Sci.* **2013**, *276*, 347–358. [CrossRef]
2. Meyer, B.K.; Polity, A.; Reppin, D.; Becker, M.; Hering, P.; Klar, P.J.; Sander, T.; Reindl, C.; Benz, J.; Eickhoff, M.; et al. Binary copper oxide semiconductors: From materials towards devices. *Phys. Status Solidi B* **2012**, *248*, 1487–1509. [CrossRef]
3. Padmadevi, B.; Pugazhendhi, A.; Khalifa, A.S.; Shanmuganathan, R.; Kalaivani, T. Novel MnO_2-CuO-BaO metal oxide nanocomposite for high performance supercapacitors. *Process. Biochem.* **2021**, *110*, 176–180. [CrossRef]
4. Hesabizadeh, T.; Jebari, N.; Madouri, A.; Hallais, G.; Clark, T.E.; Behura, S.K.; Herth, E.; Guisbiers, G. Electric-Field-Induced Phase Change in Copper Oxide Nanostructures. *ACS Omega* **2021**, *6*, 33130–33140. [CrossRef] [PubMed]
5. Sayyed, S.G.; Shaikh, A.V.; Shinde, U.P.; Hiremath, P.; Naik, N. Copper oxide-based high-performance symmetric flexible supercapacitor: Potentiodynamic deposition. *J. Mater. Sci. Mater. Electron.* **2023**, *34*, 1361. [CrossRef]
6. Barchiesi, D.; Gharbi, T.; Cakir, D.; Anglaret, E.; Fréty, N.; Kessentini, S.; Maâlej, R. Performance of Surface Plasmon Resonance Sensors Using Copper/Copper Oxide Films: Influence of Thicknesses and Optical Properties. *Photonics* **2022**, *9*, 104. [CrossRef]
7. Choudhary, S.; Sarma, J.V.N.; Pande, S.; Ababou-Girard, S.; Turban, P.; Lepine, B.; Gangopadhyay, S. Oxidation mechanism of thin Cu films: A gateway towards the formation of single oxide phase. *AIP Adv.* **2018**, *8*, 055114. [CrossRef]
8. Barchiesi, D.; Cakir, D.; Grosges, T.; Fréty, N.; Anglaret, E. Recovering effective thicknesses and optical properties of copper and copper oxide layers from absorbance measurements. *Opt. Mater.* **2019**, *91*, 138–146. [CrossRef]
9. Piskulich, Z.A.; Mesele, O.O.; Thompson, W.H. Activation Energies and Beyond. *J. Phys. Chem. A* **2019**, *123*, 7185–7194. [CrossRef]

10. Zhu, Q.; Zou, L.; Zhou, G.; Saidi, W.A.; Yang, J.C. Early and transient stages of Cu oxidation: Atomistic insights from theoretical simulations and in situ experiments. *Surf. Sci.* **2016**, *652*, 98–113. [CrossRef]
11. Zhu, Q.; Saidi, W.A.; Yang, J.C. Step-Edge Directed Metal Oxidation. *J. Phys. Chem. Lett.* **2016**, *7*, 2530–2536. [CrossRef] [PubMed]
12. Rau, J.S.; Balachandran, S.; Schneider, R.; Gumbsch, P.; Gault, B.; Greiner, C. High diffusivity pathways govern massively enhanced oxidation during tribological sliding. *Acta Mater.* **2021**, *221*, 117353. [CrossRef]
13. Mimura, K.; Jae Won, L.; Isshiki, M.; Zhu, Y.; Jiang, Q. Brief review of oxidation kinetics of copper at 350 °C to 1050 °C. *Metall. Mater. Trans. A* **2006**, *37*, 1231–1237. [CrossRef]
14. Gao, W.; Gong, H.; He, J.; Thomas, A.; Chan, L.; Li, S. Oxidation behaviour of Cu thin films on Si wafer at 175–400 °C. *Mater. Lett.* **2001**, *51*, 78–84. [CrossRef]
15. Derin, H.; Kantarli, K. Optical characterization of thin thermal oxide films on copper by ellipsometry. *Appl. Phys. A* **2002**, *75*, 391–395. [CrossRef]
16. Lee, W.J.; Wang, X.J. Structural, Optical, and Electrical Properties of Copper Oxide Films Grown by SILAR Method with Post-Annealing. *Coatings* **2021**, *11*, 864. [CrossRef]
17. Nerle, U.; Rabinal, M.H.K. Thermal Oxidation of Copper for Favorable Formation of Cupric Oxide (CuO) Semiconductor. *IOSR J. Appl. Phys.* **2013**, *5*, 1–7. [CrossRef]
18. Erdoğan, I.Y.; Güllü, O. Optical and structural properties of CuO nanofilm: Its diode application. *J. Alloy. Compd.* **2010**, *492*, 378–383. [CrossRef]
19. Belousov, V.V.; Klimashin, A.A. Catastrophic Oxidation of Copper: A Brief Review. *Metall. Mater. Trans. A* **2012**, *43*, 3715–3723. [CrossRef]
20. Jos, B.; Babu, C.R.; Shaji, S.; Anila, E.I. Study of the structural, optical, electrical and electrochemical properties of copper oxide thin films synthesized by spray pyrolysis. *J. Mater. Sci. Mater. Electron.* **2024**, *35*, 233. [CrossRef]
21. Cakir, D. Enhanced Raman Signatures on Copper Based-Materials. Ph.D. Thesis, Université de Montpellier, Montpellier, France, 2017. Available online: https://theses.hal.science/tel-01944233 (accessed on 12 March 2024).
22. Uhlig, H.H. Initial oxidation rate of metals and the logarithmic equation. *Acta Metall.* **1956**, *4*, 541–554. [CrossRef]
23. Wagner, C.; Grünewald, K. Beitrag zur Theorie des Anlauf Vorganges. III. *Z. Phys. Chem.* **1938**, *40B*, 455–475. [CrossRef]
24. Cabrera, N.; Mott, N.F. Theory of the oxidation of metals. *Rep. Prog. Phys.* **1949**, *12*, 163. [CrossRef]
25. Batiot, B.; Rogaume, T.; Richard, F.; Luche, J.; Collin, A.; Guillaume, E.; Torero, J.L. Origin and Justification of the Use of the Arrhenius Relation to Represent the Reaction Rate of the Thermal Decomposition of a Solid. *Appl. Sci.* **2021**, *11*. [CrossRef]
26. Tarantola, A. *Inverse Problem Theory and Methods for Model Parameter Estimation*; Society for Industrial and Applied Mathematics: Philadelphia, PA, USA, 2005. [CrossRef]
27. Shi, Y.; Eberhart, R. Empirical study of particle swarm optimization. In Proceedings of the 1999 Congress on Evolutionary Computation-CEC99 (Cat. No. 99TH8406), Washington, DC, USA, 6–9 July 1999; Volume 3, pp. 1945–1950. [CrossRef]
28. Barchiesi, D. The Lycurgus Cup inverse problem using photographs for characterization of matter. *J. Opt. Soc. Am. A* **2015**, *32*, 1544–1555. [CrossRef]
29. Lawless, K.R. The oxidation of metals. *Rep. Prog. Phys.* **1974**, *37*, 231. [CrossRef]
30. Kusano, K.F.; Uchikoshi, M.; Mimura, K.; Isshiki, M. Low-Temperature Oxidation of Cu(100), Cu(110) and Cu(111). *Oxid. Met.* **2014**, *82*, 181–193. [CrossRef]
31. Rhodin, T.N.J. Low Temperature Oxidation of Copper. I. Physical Mechanism1a. *J. Am. Chem. Soc.* **1950**, *72*, 5102–5106. [CrossRef]
32. Ramirez, M.; Henneken, L.; Virtanen, S. Oxidation kinetics of thin copper films and wetting behaviour of copper and Organic Solderability Preservatives (OSP) with lead-free solder. *Appl. Surf. Sci.* **2011**, *257*, 6481–6488. [CrossRef]
33. Rauh, M.; Wißmann, P. The oxidation kinetics of thin copper films studied by ellipsometry. *Thin Solid Film.* **1993**, *228*, 121–124. [CrossRef]
34. Szirtes, T.; Rózsa, P. (Eds.) CHAPTER 6—DIMENSIONAL HOMOGENEITY. In *Applied Dimensional Analysis and Modeling*, 2nd ed.; Butterworth-Heinemann: Burlington, NJ, USA, 2007; pp. 99–132. [CrossRef]
35. Roy, S.K.; Sircar, S.C. A critical appraisal of the logarithmic rate law in thin-film formation during oxidation of copper and its alloys. *Oxid. Met.* **1981**, *15*, 9–20. [CrossRef]
36. Aromaa, J.; Kekkonen, M.; Mousapour, M.; Jokilaakso, A.; Lundström, M. The Oxidation of Copper in Air at Temperatures up to 100 °C. *Corros. Mater. Degrad.* **2021**, *2*, 625–640. [CrossRef]
37. Su, M.; Cao, J.; Tian, X.; Zhang, Y.; Zhao, H. Mechanism and kinetics of Cu2O oxidation in chemical looping with oxygen uncoupling. *Proc. Combust. Inst.* **2019**, *37*, 4371–4378. [CrossRef]
38. Maack, B.; Nilius, N. Morphological and Kinetic Insights into Cu_2O–CuO Oxidation. *Phys. Status Solidi* **2020**, *257*, 1900365. [CrossRef]
39. Piippo, J.; Saario, T.; Laitinen, T.; Bojinov, M.; Hinttala, J. Electrical Properties of Surface Films Formed on Copper. In *Materials Science Forum*; Trans Tech Publications Ltd.: Wollerau, Switzerland, 1998; Volume 289–292. pp. 429–438. [CrossRef]
40. Kessentini, S.; Barchiesi, D. Convergence criteria for the particle swarm optimization in a full iterative process. In Proceedings of the 2017 IEEE Congress on Evolutionary Computation (CEC), Donostia, Spain, 5–8 June 2017; pp. 876–881. [CrossRef]
41. Clerc, M.; Kennedy, J. The particle swarm—Explosion, stability, and convergence in a multidimensional complex space. *IEEE Trans. Evol. Comput.* **2002**, *6*, 58–73. [CrossRef]
42. Figueiredo, V.; Elangovan, E.; Gonçalves, G.; Barquinha, P.; Pereira, L.; Franco, N.; Alves, E.; Martins, R.; Fortunato, E. Effect of post-annealing on the properties of copper oxide thin films obtained from the oxidation of evaporated metallic copper. *Appl. Surf. Sci.* **2008**, *254*, 3949–3954. [CrossRef]

43. Yabuki, A.; Tanaka, S. Oxidation behavior of copper nanoparticles at low temperature. *Mater. Res. Bull.* **2011**, *46*, 2323–2327. [CrossRef]
44. O'Reilly, M.; Jiang, X.; Beechinor, J.; Lynch, S.; NíDheasuna, C.; Patterson, J.; Crean, G. Investigation of the oxidation behaviour of thin film and bulk copper. *Appl. Surf. Sci.* **1995**, *91*, 152–156. [CrossRef]
45. Iijima, J.; Lim, J.W.; Hong, S.H.; Suzuki, S.; Mimura, K.; Isshiki, M. Native oxidation of ultra high purity Cu bulk and thin films. *Appl. Surf. Sci.* **2006**, *253*, 2825–2829. [CrossRef]
46. Mugwang'a, F.; Karimi, P.; Njoroge, W.; Omayio, O.; Waita, S. Optical characterization of Copper Oxide thin films prepared by reactive dc magnetron sputtering for solar cell applications. *Int. J. Thin Film. Sci. Technol.* **2013**, *2*, 15–24.
47. Raship, N.A.; Sahdan, M.Z.; Adriyanto, F.; Nurfazliana, M.F.; Bakri, A.S. Effect of annealing temperature on the properties of copper oxide films prepared by dip coating technique. *AIP Conf. Proc.* **2017**, *1788*, 030121. [CrossRef]
48. Watanabe, M.; Tomita, M.; Ichino, T. Characterization of Corrosion Products Formed on Copper in Urban, Rural/Coastal, and Hot Spring Areas. *J. Electrochem. Soc.* **2001**, *148*, B522. [CrossRef]